Biaxial Gas-Pressure Forming of a Superplastic Al_2O_3/YTZP

T.G. Nieh and J. Wadsworth

The superplastic deformation behavior of fine-grained, 20 wt% alumina/yttria-stabilized tetragonal zirconia (20 wt% Al_2O_3/YTZP) under conditions of biaxial gas-pressure deformation is described. Sheet specimens were deformed into hemispherical caps at temperatures ranging from 1450 to 1600 °C and at imposed gas pressures of 345 and 690 kPa. For the conditions examined, hemispherical caps were formed at times ranging from 10^3 to 2.1×10^4 s. The correlation between data obtained in uniaxial tensile testing and the behavior observed during the biaxial deformation experiments of this study is discussed.

Keywords:
ceramic composite, fine-grained size, forming, superplasticity, zirconia

1. Introduction

SINCE it was initially reported in 1986 (Ref 1), the science of ceramic superplasticity has rapidly advanced. A variety of ceramic materials has been shown to exhibit superplastic behavior; these include yttria-stabilized tetragonal zirconia polycrystal (Ref 1-3), alumina (Ref 4), silicon nitride (Ref 4), hydroxyapatite (Ref 5), and composites of alumina-zirconia (Ref 6) and silicon nitride-silicon carbide (Ref 7). For the most part, reports of ceramic superplasticity to date have focused on acquiring a fundamental understanding of ceramic superplasticity through uniaxial tension or compression testing. These studies have yielded invaluable information on the deformation behavior (e.g., strain rate sensitivity or stress exponent) and microstructural evolution (e.g., concurrent grain growth and cavitation behavior) of superplastic ceramics (Ref 8, 9). The knowledge of fundamental issues in ceramic superplasticity has now advanced to the stage that the technological application of superplastic deformation is beginning to receive increasing attention. Examples include successful extrusion of YTZP powders (Ref 10), closed-die deformation of YTZP (Ref 11), punch forming of YTZP sheet (Ref 12), and most recently, biaxial gas-pressure deformation of 20 wt% Al_2O_3/YTZP (Ref 13), monolithic YTZP (Ref 14), and Fe/Fe_3C (Ref 15). These forming processes offer technological advantages of greater dimensional control and increased variety and complexity of shapes than is possible with conventional ceramic shaping technology. This paper presents a description of the superplastic forming behavior of 20 wt% Al_2O_3/YTZP sheet under conditions of biaxial gas-pressure forming.

2. Material and Procedure

The material used in this study was a fine-grained YTZ containing 20 wt% Al_2O_3, (denoted Al_2O_3/YTZP, hereafter) obtained as 50-mm-diam, 1.5-mm-thick disks, from Nikkato Corp., Japan. The microstructure exhibited an equiaxed YTZP grain size of 0.5 μm with a random distribution of 0.5-μm-diam Al_2O_3 grains. Data regarding the superplastic flow properties (Ref 16), grain growth behavior (Ref 17), and cavitation characteristics (Ref 18) of this Al_2O_3/YTZP (under uniaxial tension conditions) system have previously been reported. Based on information from these previous studies, a gas-pressure forming apparatus was constructed with the capability to operate at temperatures of ≤1700 °C at gas forming pressures of ≤ 2.5 MPa. These forming pressures were chosen so as to impart true strain rates over the range of approximately 10^{-5} to 10^{-3} s^{-1}, within which Al_2O_3/YTZP exhibits the highest superplastic elongation. A detailed description of this apparatus was presented elsewhere (Ref 14).

All experiments were conducted isothermally under conditions of constant applied forming pressure. Following equilibration at the temperature of interest, the desired forming pressure was applied, and the resultant deformation was monitored. Experiments were terminated when the deformation height corresponded to that of a hemisphere. The 50-mm-diam disks were clamped about their periphery resulting in an unconstrained 38-mm-diam diaphragm. Thus, the height for deformation to a hemisphere was 19 mm.

Following deformation, all hemispheres were measured to determine the degree of deformation. These measurements were employed to determine true strain and average strain rate for each experimental condition. Strain distribution can be studied by two techniques, i.e., by sectioning formed articles or by using a grid system. The former technique is employed in the following section to describe the progressive deformation of a hemisphere. Use of the grid system involves placing an orthogonal grid system onto the undeformed diaphragm with the use of a diamond-tipped scribe and measuring the displacement of the grid subsequent to deformation. The grid technique provides reliable data on the in-plane strains with the through-thickness strains derived from these measurements through conservation of volume considerations.

3. Results and Discussion

Six Al_2O_3/YTZP superplastically hemispheres deformed are shown in Fig. 1. The hemispheres were deformed at forming pressures of 345 and 690 kPa. For the range of forming pressures and temperatures examined in this study,

T.G. Nieh and **J. Wadsworth,** Lawrence Livermore National Laboratory, P.O. Box 808, L-350, Livermore, CA 94550, USA

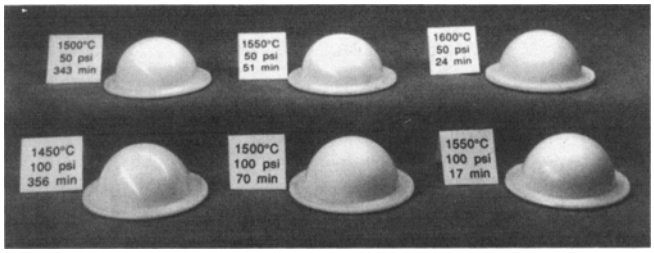

Fig. 1 Al_2O_3/YTZP hemispheres superplastically deformed at various conditions (50 psi = 340 kPa, 100 psi = 680 kPa)

Al_2O_3/YTZP disks were deformed into hemispherical caps in times ranging from 10^3 to 2×10^4 s. As expected, higher temperatures and higher forming pressures result in faster deformation times.

The superplastic forming behavior for Al_2O_3/YTZP sheet at various temperatures and pressures is summarized in the deformation-time plots of Fig. 2(a) and (b). The curves in Fig. 2 indicate that there are essentially three distinct regions of behavior as deformation progresses for all the test conditions examined. Initially, the height of the deforming dome increases quite rapidly. This stage is followed by a period of apparent steady-state deformation, which is characterized by a minimum deforming rate. Finally, as the height approaches that of a hemisphere, the deformation rate increases again.

The three-stage behavior in Fig. 2 appears to be similar to the creep curve of metal alloys deformed under a constant value of uniaxial stress, but its physical interpretation is quite different. This is because, although the applied pressure remained constant throughout the test, the resultant applied stress varies continuously during the course of deformation. In fact, the pressure-stress relationship for a deforming spherical thin shell follows the equation:

$$\sigma = \frac{P\rho}{2t} \qquad \text{(Eq 1)}$$

where σ is the principal tangential stress acting in a shell having a wall of thickness, t, and radius, ρ, and P is the applied gas pressure. For the experiments of this study, P remains constant, but ρ and t (and therefore σ) vary during the course of the test. Qualitatively, Eq 1 predicts a high flow stress at the beginning of a test when the radius is very high and at the end of a test as the thickness decreases. This results in a high forming rate at both low and high dome heights. As t and ρ are interdependent, the second stage of deformation occurs at a more-or-less constant rate because a decreasing radius is balanced by a decreasing shell thickness. Therefore, the three-stage behavior observed in Fig. 2 not only results from the creep of the material, but also from the nature of biaxial forming.

To provide a more quantitative description of the relationship between σ, shell deformation, and strain rate, a mechanical analysis of the deformation process was performed. By assuming that the volume of the deforming shell remains constant and that the thickness of the shell decreases uniformly during deformation, the flow stress acting in the shell may be determined through Eq 1. For the present experiments, the radius was deduced from the height of the deforming shell as measured and deduced from the contact linear variable differential transformer (LVDT) sensor. The height of a deforming hemispherical cap may be related to its radius through a consideration of the cap geometry, as schematically shown in Fig. 3.

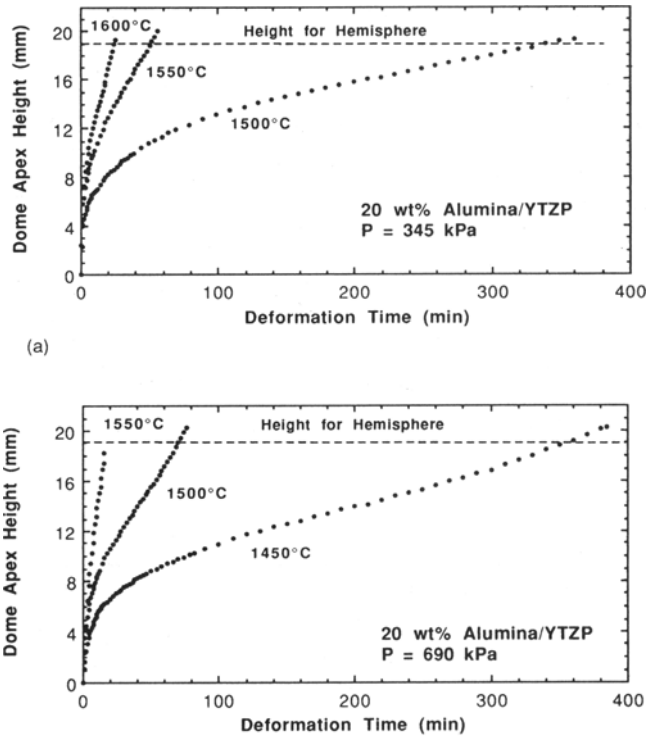

Fig. 2 Superplastic forming behavior of Al_2O_3/YTZP sheet at (a) 345 kPa and (b) 690 kPa gas pressures

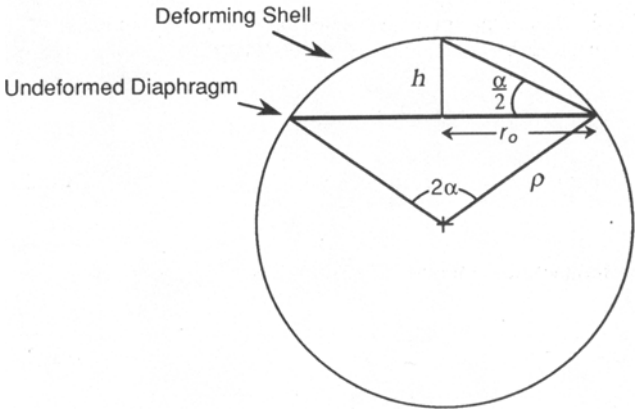

Fig. 3 A hemispherical cap of height h and base radius r_o may be considered to be a section of a sphere of radius ρ and included angle 2α

A hemispherical cap of apex height, h, and base radius of r_o, may be considered as a section of a sphere of radius ρ and included angle 2α. The included half-angle α may be determined by measuring the height h of the cap:

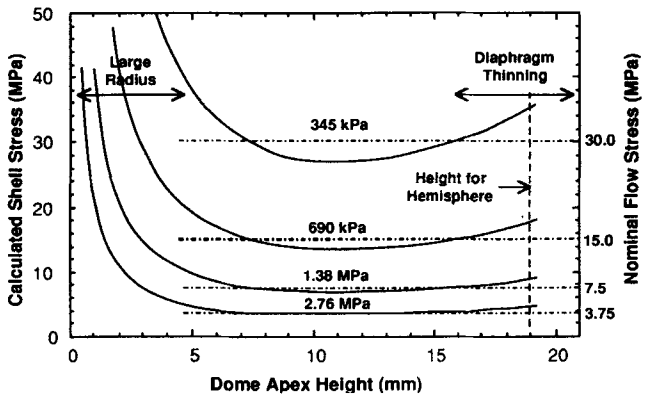

Fig. 4 The relationship between σ and dome apex height

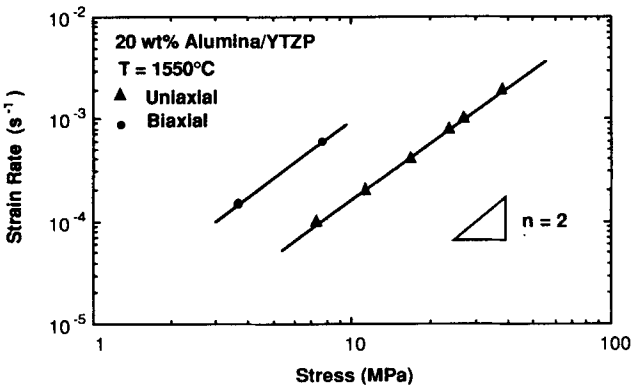

Fig. 6 A direct comparison between the strain rate-stress data obtained from the present biaxial forming experiments at 1550 °C and those from uniaxial tests

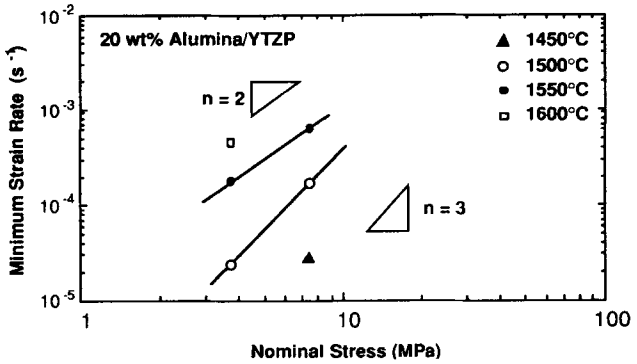

Fig. 5 Minimum strain rate versus nominal stress for biaxial gas-pressure forming of 20 wt% Al_2O_3/YTZP

$$\tan\left(\frac{\alpha}{2}\right) = \frac{h}{r_o} \qquad \text{(Eq 2)}$$

The radius ρ may then be determined as:

$$\rho = \frac{r_o}{\sin \alpha} \qquad \text{(Eq 3)}$$

Knowledge of ρ and h together with the assumption that volume is conserved enables a determination of the average shell thickness $\bar{t}$:

$$\bar{t} = \frac{r_o^2 t_o}{2\rho h} \qquad \text{(Eq 4)}$$

Equations 1 through 4 establish a relationship between the height of a deforming hemispherical shell and the flow stress acting in the shell wall.

For the present testing conditions, the relationship between σ and dome apex height has been calculated and is shown in Fig. 4. For these calculations, the initial thickness, t, was 1.5 mm, and the base radius, r_o, was 19 mm. Note in Fig. 4 that for each forming pressure, there exists a region in which a nominal flow stress acts for a large portion of the test. This region corresponds to the aforementioned steady-state deformation region observed in the deformation-time plots (Fig. 2). The computed results presented in Fig. 4 show that the nominal flow stresses for the experiments of this study were approximately 3.75 and 7.5 MPa for applied gas pressures of 345 and 690 kPa, respectively. Effective stresses are higher for a large radius (in the initial stages of forming) and diaphragm thinning (in the final stages of forming) regions. These calculations of variation in flow stress with increasing dome height agree with the general description of variation in deformation rate with increasing dome height, shown in Fig. 2.

In addition to the computed flow stresses for each experiment, the deformation strain rates were also estimated. As noted in Fig. 2, the steady-state deformation region also corresponds to the minimum strain rate region. The determination of this steady-state strain rate as a function of the nominal stress, therefore, provides a first-order result of the biaxial forming properties. This is presented graphically as a log-log plot in Fig. 5. Assuming a conventional power-law relationship, the minimum strain rate, $\dot{\varepsilon}$, can be expressed as:

$$\dot{\varepsilon} = B \cdot \sigma^n \qquad \text{(Eq 5)}$$

where σ is the nominal stress, n is the stress exponent, and B is a constant. Despite limited data, the n value is approximately 2 to 3, which is in the range for superplastic ceramics. Specifically, n is ~3 at 1500 °C, but decreases to ~2 at 1550 °C.

It is of interest to compare the present results with those from uniaxial tests. Shown in Fig. 6 is a direct comparison between the strain rate-stress data obtained from the present biaxial forming experiments at 1550 °C and those from uniaxial tests (Ref 16). It is particularly pointed out that the nominal stress, or stress for the biaxial tests used in Fig. 5, is in fact the tangential stress. For the case of biaxial forming and in the case of a spherical dome, the stress, as used in Fig. 6, acting on the dome apex is the resultant stress of the tangential and circumferential stresses, which equals $\sqrt{2}$ of the stress value indicated in Fig. 5. Taking into account this resultant stress would shift the data in Fig. 6 for the biaxial tests downward, thus moving

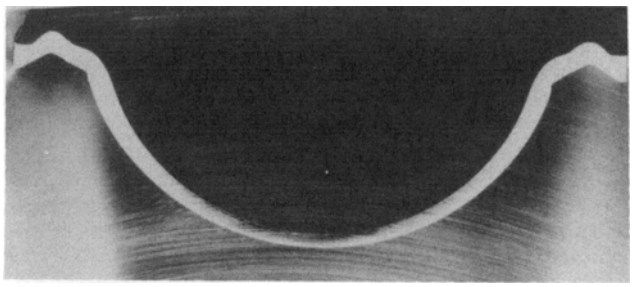

Fig. 7 Cross section of a dome deformed at 1550 °C

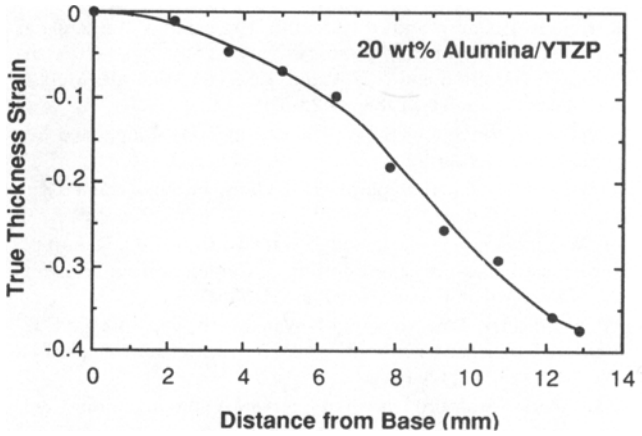

Fig. 8 Strain distributions for the disk deformed at 1550 °C and 690 kPa pressure

them closer to the data for the uniaxial tests. However, the strain rate from the biaxial forming test is still approximately 3 to 4 times faster than that from the uniaxial tests. A faster strain rate was also observed during the biaxial gas-pressure forming of YTZP (Ref 14). In fact, in the case of YTZP, the strain rate from the biaxial forming test is also approximately 3 to 4 times faster than those from the uniaxial tests.

Shown in Fig. 7 is the cross section of a dome deformed at 1550 °C. As expected, the thickness of the dome at each location varies. The thickness nonuniformity primarily arises from the variation in stress state from the clamped periphery of the diaphragm to its freely deforming center. At the center of the diaphragm is a stress state of equibiaxial tension (plane stress) described fully by Eq 1. At the clamped periphery of the diaphragm, however, is a state of plane strain. When the diaphragm is deformed by an applied gas pressure, the state of stress varies between the apex and the periphery. As a result of this stress gradient, deformation occurs under a corresponding strain rate gradient. The degree of thickness variation is determined by both the local stress and the strain rate sensitivity, $m = 1/n$, of the deforming sheet. In the present case, thickness strain distributions of the deformed disk are shown in Fig. 8. The thickness of the periphery of the diaphragm is 1.5 mm, and the thickness of the apex is only ~1.0 mm.

Cornfield and Johnson (Ref 19) developed a model to predict the thickness distribution for biaxial bulge forming. The model was, however, derived under the condition of a constant m value, which is invalid for most superplastic ceramics. It has been reported that many superplastic ceramics, as a result of a fine grain size, undergo severe dynamic grain growth during superplastic deformation, which changes the m value (Ref 8, 9, 20). Therefore, a kinematic equation that incorporates dynamic grain growth effects must be ultimately developed in order to predict precisely the strain distribution.

4. Conclusions

A fine-grained 20 wt% Al_2O_3/YTZP was successfully formed using a biaxial gas-pressure forming technique. Sheet specimens were deformed into hemispherical caps at temperatures ranging from 1450 to 1600 °C and at imposed gas pressures of 345 and 690 kPa. For the forming conditions examined, hemispherical caps were formed at times ranging from 10^3 to 2.1×10^4 s. Mechanical analyses of the deformation process indicate that the stress exponent for deformation is approximately 2 to 3. The strain rate from the biaxial forming test is approximately 3 to 4 times faster than that from the uniaxial tests, which is similar to that observed during the biaxial forming of YTZP. The deformed domes exhibited a thickness variation from the dome apex to dome base.

Acknowledgment

Part of this work was performed under the auspices of the U.S. Department of Energy by LLNL under contract No. W-7405-Eng-48. The financial support was provided by the Army Research Office. The authors wish to thank Dr. J.P. Wittenauer for his technical contributions and for carrying out the gas pressure forming tests.

References

1. F. Wakai, S. Sakaguchi, and Y. Matsuno, Superplasticity of Yttria-Stabilized Tetragonal ZrO_2 Polycrystals, *Adv. Ceram. Mater.*, Vol 1 (No. 3), 1986, p 259-263
2. T.G. Nieh and J. Wadsworth, Superplastic Behavior of a Fine-Grained, Yttria-Stabilized, Tetragonal Zirconia Polycrystal (YTZP), *Acta Metall.*, Vol 38, 1990, p 1121-1133
3. T. Hermansson, K.P.D. Lagerlof, and G.L. Dunlop, Superplastic Deformation of YTZP Zirconia, *Superplasticity and Superplastic Forming*, C.H. Hamilton and N.E. Paton, Ed., The Minerals, Metals, and Materials Society, 1988, p 631-635
4. I.W. Chen and L.A. Xue, Superplastic Alumina Ceramics with Grain Growth Inhibitors, *J. Am. Ceram. Soc.*, Vol 73 (No. 9), 1990, p 2585-2609
5. F. Wakai, Y. Kodama, S. Sakaguchi, and T. Nonami, Superplasticity of Hot Isostatically Pressed Hydroxyapatite, *J. Am. Ceram. Soc.*, Vol 73 (No. 2), 1990, p 257-260
6. T.G. Nieh, C.M. McNally, and J. Wadsworth, Superplastic Behavior of a 20% Al_2O_3/YTZ Ceramic Composite, *Scr. Metall.*, Vol 23, 1989, p 457-460
7. F. Wakai, Y. Kodama, S. Sakaguchi, N. Murayama, K. Izaki, and K. Niihara, A Superplastic Covalent Crystal Composite, *Nature*, Vol 344, 1990, p 421-423
8. T.G. Nieh and J. Wadsworth, Dynamic Grain Growth in Yttria-Stabilized Tetragonal Zirconia during Superplastic Deformation, *J. Am. Ceram. Soc.*, Vol 72 (No. 8), 1989, p 1469-1472
9. D.J. Schissler, A.H. Chokshi, T.G. Nieh, and J. Wadsworth, Microstructural Aspects of Superplastic Tensile Deformation and Cavitation Failure in a Fine-Grained, Yttria Stabilized, Tetragonal Zirconia, *Acta Metall. Mater.*, Vol 29 (No. 12), 1991, p 3227-3236

10. B. Kellett, P. Carry, and A. Mocellin, Extrusion of Tet-ZrO_2 at Elevated Temperatures, *Superplasticity and Superplastic Forming*, C.H. Hamilton and N.E. Paton, Ed., The Minerals, Metals, and Materials Society, 1988, p 625-630
11. F. Wakai, A Review of Superplasticity in ZrO_2-Toughened Ceramics, *Brit. Ceram. Trans. J.*, Vol 88, 1989, p 205-208
12. X. Wu and I.W. Chen, Superplastic Bulging of Fine-Grained Zirconia, *J. Am. Ceram. Soc.*, Vol 73 (No. 3), 1990, p 746-749
13. J.P. Wittenauer, T.G. Nieh, and J. Wadsworth, A First Report on Superplastic Gas-Pressure Forming of Ceramic Sheet, *Scr. Metall. Mater.*, Vol 26 (No. 4), 1992, p 551-556
14. J.P. Wittenauer, T.G. Nieh, and J. Wadsworth, Superplastic Gas-Pressure Deformation of YTZP Sheet, *J. Am. Ceram. Soc.*, Vol 76 (No. 8), 1993, p 1665-1672
15. O.D. Sherby, Stanford University, private communication, 1993
16. T.G. Nieh and J. Wadsworth, Superplasticity in Fine-Grained 20%Al_2O_3/YTZ Composite, *Acta Metall. Mater.*, Vol 39, 1991, p 3037-3045
17. T.G. Nieh, C.M. Tomasello, and J. Wadsworth, Dynamic Grain Growth in Superplastic Ceramics and Ceramic Composites, Symposium on *Superplasticity in Metals, Ceramics, and Intermetallics*, MRS Proceeding No. 196, M.J. Mayo, M. Kobayashi, and J. Wadsworth, Ed., The Materials Research Society, 1990, p 343-348
18. A. Chokshi, D.J. Schissler, T.G. Nieh, and J. Wadsworth, A Comparative Study of Superplastic Deformation and Cavitation Failure in a Yttria Stabilized Zirconia and a Zirconia Alumina Composite, Symposium on *Superplasticity in Metals, Ceramics, and Intermetallics*, MRS Proceeding No. 196, M.J. Mayo, M. Kobayashi, and J. Wadsworth, Ed., The Materials Research Society, 1990, p 379-384
19. G.C. Cornfield and R.H. Johnson, The Forming of Superplastic Sheet Metal, *Int. J. Mech. Sci.*, Vol 12, 1970, p 479-490
20. L.A. Xue and R. Raj, Superplastic Deformation of Zinc Sulfide near Transformation Temperature (1020 °C), *J. Am. Ceram. Soc.*, Vol 72, 1989, p 1792-1796